PHYSICAL REVIEW MATERIALS **4**, 055002 (2020)

Editors' Suggestion

Monoclinic semimetal IrSi synthesized under high pressure above 25 GPa: Crystal structure, electronic, and magnetic properties

Y. Fujishiro,[1] N. Kanazawa,[1] T. Shinmei,[2] M. Nishi,[2] T. Nakajima,[1,4,*] T. Arima,[3,4] D. Hashizume,[4] M. S. Bahramy,[1] T. Irifune,[2] and Y. Tokura[1,4,5]

[1] *Department of Applied Physics and Quantum-Phase Electronics Center (QPEC), University of Tokyo, Tokyo 113-8656, Japan*
[2] *Geodynamics Research Center, Ehime University, Ehime 790-8577, Japan*
[3] *Department of Advanced Materials Science, The University of Tokyo, Kashiwa, Chiba 277-8561, Japan*
[4] *RIKEN Center for Emergent Matter Science (CEMS), Wako 351-0198, Japan*
[5] *Tokyo College, University of Tokyo, Tokyo 113-8656, Japan*

(Received 10 February 2020; accepted 23 April 2020; published 15 May 2020)

We have synthesized a monoclinic phase of IrSi by means of high-pressure and high-temperature treatment above 25 GPa, whereas the theoretically predicted high-pressure phase (i.e., FeSi-type structure) was not identified up to 48 GPa. Magnetotransport measurements clarify the semimetallic nature (carrier density of $\sim 6-9\times 10^{19}/\mathrm{cm}^3$) of monoclinic IrSi, in agreement with our band structure calculations. Furthermore, the surface electronic bands are predicted to show the large Rashba spin splitting, offering potential spintronic applications of this material.

DOI: 10.1103/PhysRevMaterials.4.055002

Transition metals and group-14 elements form a large family of intermetallic compounds, which have been intensively studied in terms of fundamental science and technological applications. In particular, transition metal monosilicides (MSi, $M =$ transition metal) exhibit diverse physical properties and functionalities varying with their crystal structures [1–3], which can be either CrB-type ($M =$ Sc,Y,Zr), FeB-type ($M =$ La, Ti, Zr, Hf), FeSi-type ($M =$ Cr, Mn,Te,Re,Fe,Ru,Os,Co,Rh), CsCl-type ($M =$ Ru), or MnP-type ($M =$ Rh, Ir, Ni, Pd, Pt). For instance, FeSi-type MSi have attracted much attention for topological magnetic and electronic structures, such as magnetic skyrmions (e.g., MnSi, $\mathrm{Fe}_{1-x}\mathrm{Co}_x\mathrm{Si}$, $\mathrm{Mn}_{1-x}\mathrm{Fe}_x\mathrm{Si}$) [4–6] and unconventional fermions with large Chern number (e.g., CoSi, RhSi) [7–11]. Meanwhile, MnP-type MSi [space group *Pnma* (No. 62)] has been used in Si microelectronics, especially for ohmic contacts and Shottky barrier devices (e.g., PtSi, NiSi, IrSi) [12–14]. The electronic band structures seem to be directly linked to the crystal structures in MSi [1], and therefore, it would be of great importance to explore their various phases, which may give rise to characteristic physical properties.

In this context, high-pressure synthesis is a powerful technique to explore various phases of matter by transforming potential-energy landscapes. It generally enables the isolation of densely packed structures that are not accessible at ambient pressures [15–17]. Accordingly, the distinct changes in electronic and magnetic properties are expected, as induced by the modification in the electron band structure around the Fermi energy in MSi [1,15].

IrSi adopts MnP-type structure at ambient pressure [2,3,15], while its high-pressure stability remains largely elusive. A theoretical study has predicted the phase transition into FeSi-type structure at 25 GPa [15], which is typically a denser structure than MnP-type structure [15–17]. The coordination number of transition metals is also increased from sixfold (MnP-type) to sevenfold (FeSi-type) [15]. In addition, electronic properties are expected to change from metallic (MnP-type) to semimetallic (FeSi-type) [15], suggesting the emergence of unconventional topological fermions [7–11] in FeSi-type IrSi associated with large relativistic spin-orbit coupling.

Contrary to the initial expectation, however, we have discovered that IrSi crystallizes into a monoclinic structure with space group $P2_1/c$ (No. 14) at high pressure. This unexplored monoclinic phase is stabilized by the high-pressure–high temperature (HPHT) treatment, at least for a pressure range of 25–48 GPa, and is recoverable after decompression and thermal quenching. In this paper, we report the crystal structure refinements as well as the electronic and magnetic properties of monoclinic IrSi. The identified semimetallic electronic properties of monoclinic IrSi is supported by the band structure calculations.

The IrSi alloy ingot was first prepared by melting the elements with the stoichiometry ratio in an arc furnace under argon atmosphere. The HPHT treatment was performed by using multianvil high-pressure apparatus named ORANGE-3000 (for applying pressures up to 25 GPa) and MADONNA-II (for applying 48 GPa) installed at Geodynamics Research Center in Ehime University. After keeping HPHT conditions (for detailed conditions, see Table I) for 1 h, the samples were quenched to room temperature, followed by a release of pressure. Powder x-ray diffraction (XRD) measurements were performed with a Rigaku RINT TTR-III using Cu Kα

---

[*] Present address: Institute for Solid State Physics, The University of Tokyo, Kashiwa, Chiba 277-8561, Japan.

TABLE I. Experimental conditions for high-pressure and high-temperature treatment, as well as the consequent phases obtained for IrSi.

Sample	Pressure (GPa)	Temperature (°C)	Crystal structure
#1	0	Arc melted	Orthorohmbic (MnP-type)
#2	17	800	
#3	25	800	Monoclinic
#4	25	1300	
#5	48	800	

radiation, except for the sample synthesized at 25 GPa and 800 °C where the XRD pattern was measured by a capillary method by a Rigaku SmartLab diffractometer using Cu $K\alpha_1$ radiation ($\lambda = 1.54054$ Å). Crystal structure refinements were performed with the software RIETAN-FP [18].

Figure 1(a) shows the powder XRD pattern of the arc-melted sample of IrSi, which is consistent with the previously reported orthorhombic MnP-type structure [Fig. 1(b)] with space group *Pnma* (No. 62) [2,3,15]. The same powder XRD pattern was observed for the HPHT treatment at 17 GPa and 800 °C (Table I), confirming the structural stability of the orthorhombic MnP-type structure up to 17 GPa.

Meanwhile, the structural phase transition is clearly observed for the HPHT treatment above 25 GPa (Table I). Figure 1(c) shows the powder XRD pattern of the sample synthesized at 25 GPa and 800 °C, which was collected by the capillary method. Importantly, the observed XRD pattern [Fig. 1(c)] cannot be explained by any reported Ir-Si alloys, nor by the FeSi-type structure, which has been predicted theoretically as the possible high-pressure phase of IrSi [15]. Instead, we have found that the XRD pattern can be fully indexed by a monoclinic structure without any impurity phase by using the autoindex software CONOGRAPH [19]. The structural refinements were then performed with a monoclinic space group $P2_1/c$ (No. 14) [Fig. 1(d)], which was reported for RhSi under pressure [20]. The final R factors and the goodness-of-fit were $R_{\mathrm{wp}} = 1.419\%$, $R_{\mathrm{e}} = 1.147\%$, $S = 1.2366$, and $R_{\mathrm{B}} = 2.617\%$. We note that the intensity data for 2θ ranges of 104.6°–107.0°, 109.5°–112.20°, 122.0°–124.6° are excluded for the Rietveld analysis, which contain the intensity peaks arising from the measurement setups. The refined unit-cell parameters are summarized in Table II. The transition from the orthorhombic to monoclinic structure was indeed accompanied by a decrease in the unit-cell volume (i.e., increase in the density) by 2.4% [$V_{\mathrm{orthorhombic}} = 111.58(9)$ Å^3 [2] to $V_{\mathrm{monoclinic}} = 108.87(2)$ Å^3], and the monoclinic phase was stable up to 48 GPa (Table II).

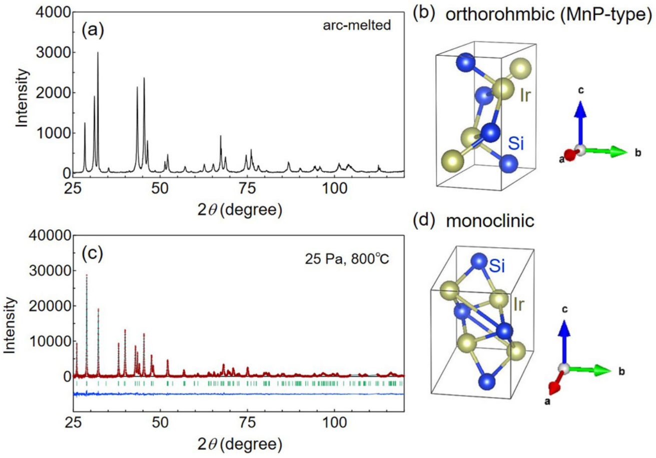

FIG. 1. Powder x-ray diffraction pattern for the arc-melted sample (a) and the sample synthesized at 25 GPa and 800 °C (c). The result of Reitveld refinement is also shown for (c), with the background intensity subtracted from the data. The refined crystal structures are shown in (b) and (d), respectively.

To confirm the relative stability of the orthorhombic (MnP-type), monoclinic, and the theoretically predicted [15] cubic (FeSi-type) phases of IrSi, we systematically studied their volumetric properties within density functional theory using Perdew-Burke-Ernzerhof exchange-correlation functional as implemented in the VASP program [21,22]. The sampling of the Brillouin zone was done by 1000 homogeneously spaced k points. For a given unit cell volume (V), the lattice parameters and atomic positions were optimized until the magnitude of the force on each ion became less than 0.001 eV/Å. We note that the optimized lattice parameters (not shown) for monoclinic IrSi are nearly identical to the result of the Rietveld analysis. The resulting total energies $E(V)$ is shown in Fig. 2(a), revealing that the theoretically predicted FeSi-type cubic phase [15] is energetically less stable than the monoclinic phase for volume compressions down to nearly 15%. This implies that under the application of hydrostatic pressure, the monoclinic phase transition precedes that of the FeSi-type cubic phase. To confirm this, we fitted the calculated $E(V)$ with the third-order Birch-Murnaghan equation [23–25] to estimate the transition pressure P_T, defined as the common tangent between the fitted $E(V)$ curves. As shown in Fig. 2(b), the transition pressure for the FeSi-type cubic structure ($P_{\mathrm{OC}} = 19.5$ GPa) is reassuringly higher than that of the experimentally realized monoclinic structure ($P_{\mathrm{OM}} = 14.8$ GPa). The common tangents of $E(V)$ curves provide intuitive insight into the enthalpy of these three phases as well. Having the enthalpy defined as $H = E + PV$, a common tangent corresponds to a line that connects two points in the $E - V$ space with the same H, i.e., $\Delta H = \Delta E + P\Delta V = 0$. Hence, the enthalpies of the orthorhombic and monoclinic phases must cross each other ($\Delta H = H_{\mathrm{o}} - H_{\mathrm{M}} = 0$) at P_{OM}, while such a crossover between orthorhombic and cubic phases ($\Delta H = H_{\mathrm{o}} - H_{\mathrm{c}} = 0$) must occur at P_{OC}. Indeed, a direct calculation of the enthalpy proves this as shown in Fig. 2(c). The fact that $P_{\mathrm{OM}} < P_{\mathrm{OC}}$ guarantees $H_{\mathrm{M}} < H_{\mathrm{C}}$. This accordingly means that the system needs less thermodynamic work $P\Delta V$ to transform into the monoclinic phase than it does for transition to the FeSi-type cubic structure.

Figures 3(b) and 3(c) show the electronic band structure and the density of states (DOS) for the monoclinic IrSi, with

TABLE II. Space groups, unit-cell parameters, atomic positions, and isotropic B factors of orthorhombic IrSi (cited from Ref. [2]) and monoclinic IrSi refined by Rietveld analysis. The number of Ir or Si atoms in the unit cell is four for both phases.

Phase	Space group	a (Å)	b (Å)	c (Å)	α, β, γ (°)	Atom	Position	x	y	z	B_{iso} (Å^2)
Orthorhmbic	$Pnma$	5.5460(3)	3.21505(14)	6.2576(3)	$\alpha=\beta=\gamma=90$	Ir	4c	−0.0047(7)	0.25000	0.2029(3)	0.96(4)
						Si	4c	0.174(2)	0.25000	0.577(2)	0.4(2)
Monoclinic	$P2_1/c$	4.6115(5)	4.5385(4)	5.6962(6)	$\alpha = \gamma = 90$	Ir	4e	0.2963(2)	0.8603(1)	0.1297(1)	0.33(2)
					$\beta=114.051(5)$	Si	4e	0.791(1)	0.8603(8)	0.5489(5)	0.66(7)

its Brillouin zone and corresponding high symmetry k-points being illustrated in Fig. 3(a). As shown in Fig. 3(b), there is a small overlap between conduction and valence bands at the Fermi energy forming hole and electron pockets, suggesting a compensated semimetallic behavior for the monoclinic IrSi. The pseudogap formation is also observed around the Fermi energy, where the main contribution to DOS is dominated by the Ir atom [Fig. 3(c)].

The magnetic and electrical transport properties of monoclinic IrSi are summarized in Fig. 4. Diamagnetism with a magnetic susceptibility -8.79×10^{-4} emu/mol (300 K) is observed with almost no temperature dependence [Fig. 4(a)]. By subtracting the diamagnetic contribution from the elements [26], the valence-electron driven diamagnetism of IrSi is obtained as -5.79×10^{-4} emu/mol. This value is relatively large, being about one-third of the diamagnetic susceptibility of Bi, which is the representative semimetal exhibiting large diamagnetism [27,28]. This may indicate the importance of the interband contribution [28] to the diamagnetism via large spin-orbit coupling being typical of heavy-element (e.g., Ir) based semimetals.

The resistivity ρ_{xx} shows a metallic behavior with little temperature dependence as shown in Fig. 4(b). Also, a positive magnetoresistivity (10% at 10 T) is observed with an applied magnetic field perpendicular to the current (data not shown). The carrier density n ($\sim6-9\times10^{19}/\text{cm}^3$) is obtained from the Hall resistivity ρ_{yx} [Fig. 4(c)] in the isotropic single-carrier model $\rho_{yx} = B/ne$, where B and e are the magnetic field and elementary charge, respectively, being consistent with the semimetallic band structure of IrSi. The temperature dependence of the carrier density n as well as the mobility μ ($\sim$53 cm^2/Vs at 2 K) estimated from the resistivity at 0 T [$\mu = 1/(\rho_{xx}ne)$], are summarized in Fig. 4(d). We note that the presence of the minor carrier (electron) may result in the overestimation of the carrier density, leading to the underestimation of the mobility. Also, the mobility (or resistivity) in this polycrystalline form may be affected by the presence of grain boundaries and is likely underestimated.

We have also calculated the surface band structure of monoclinic IrSi, as shown in Fig. 5. For this calculation, we have constructed a large tight-binding supercell containing 60 units of IrSi stacked along the b axis. The hopping matrix elements

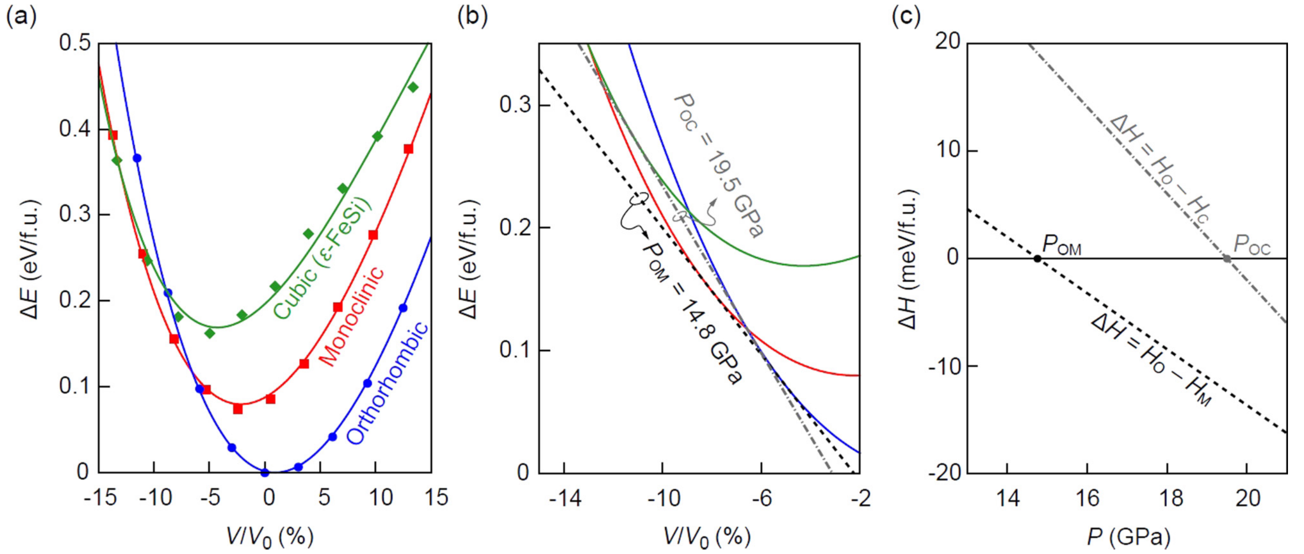

FIG. 2. (a) Volume dependence of the internal energy calculated for the orthorhombic ($Pnma$) phase (blue circles), monoclinic ($P2_1/c$) phase (red squares), and the previously predicted cubic (ε-FeSi-type) phase [15] (green diamonds). The solid lines are the corresponding equations of state $E(V)$ for these phases obtained by fitting the calculated results to the third-order Birch-Murnaghan equation. V_0 is the volume of the orthorhombic unit cell at the ambient pressure. (b) A magnified view of the equation of states. The resulting common tangent between the orthorhombic and monoclinic (cubic ε-FeSi-type) phases is shown by the black dashed line (grey dash-dotted line). Here, P_{OM} (P_{OC}) is the negative slope of the common tangent and corresponds to the pressure needed for the transition from orthorhombic to monoclinic (cubic) phase. (c) The pressure dependence of the enthalpy difference between the orthorhombic and monoclinic phase (black dashed line), compared against that between the orthorhombic and cubic phase (grey dash-dotted line).

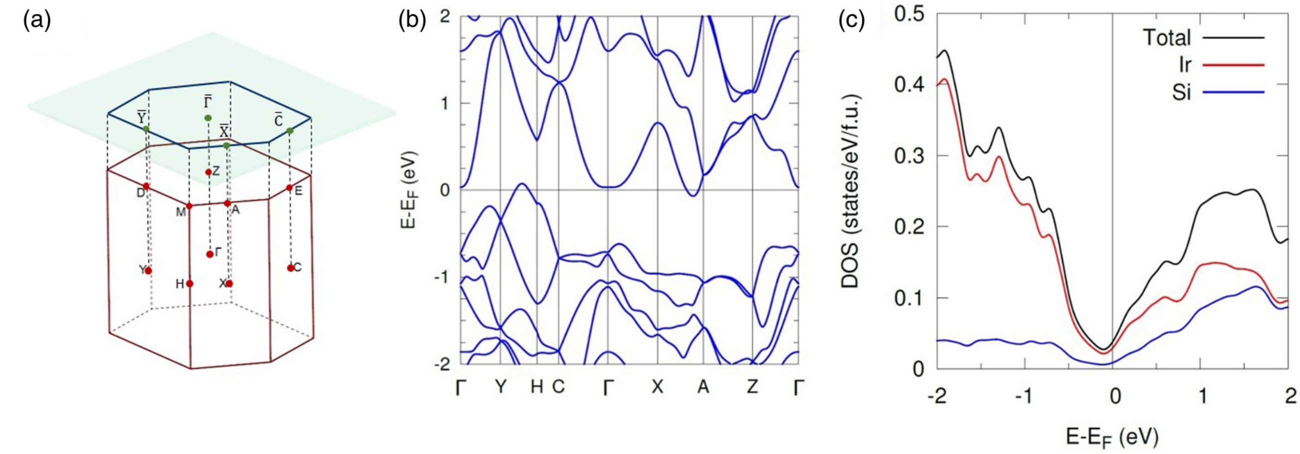

FIG. 3. Brillouin Zone (a), band structure (b), and density of states (DOS) (c) for the monoclinic IrSi. The surface projection of *k* points is denoted by the green dots in (a).

are extracted from our first-principle calculations using maximally localized Wannier functions [29]. The resulting spectral weight function is then projected onto the topmost IrSi layer. The surface band structure has finite density of states at the Fermi energy, showing a large Rashba spin splitting [30] on the order of 0.1 eV. To discuss the magnitude of the Rashba splitting in the monoclinic IrSi, we estimated the Rashba parameter α by fitting the surface band structure around the $\bar{\mathrm{Y}}$ point by $E = \frac{\hbar^2}{2m}k^2 + \alpha k$ [30]. The obtained value $\alpha = 0.9\times10^{-11}$ [eVm] is relatively large, being comparable to that of the interface of InGaAs/InAlAs ($\alpha = 0.7\times10^{-11}$ [eVm]) [31] but smaller than those of the surface states of Au(111) ($\alpha = 3.3\times10^{-11}$ [eVm]) [32] and Bi(111) ($\alpha = 5.5\times10^{-11}$ [eVm]) [33]. The broken inversion symmetry at the surface, as well as the large spin-orbit coupling from Ir, may give rise to such a large spin splitting. Given the fact that high-pressure phases can sometimes be stabilized in epitaxial films due to the strain from substrates, it would be of great interest to tailor the thin film of monoclinic IrSi, where the large Rashba spin splitting may provide versatile spintronic functionalities, such as the effective generation of spin current [34].

In conclusion, we have synthesized a high-pressure phase of IrSi, which crystallizes into the monoclinic space group $P2_1/c$ (No. 14), with no trace of theoretically predicted FeSi-type structure [15] up to 48 GPa. We speculate that this is partly due to the structural rigidity of the FeSi-type structure where the displacement of atoms is allowed only along the body diagonals of the cubic unit cell [17]. Indeed, the appearance of the FeSi-type structure as an intermediate phase in the high-pressure structural sequence can be sometimes

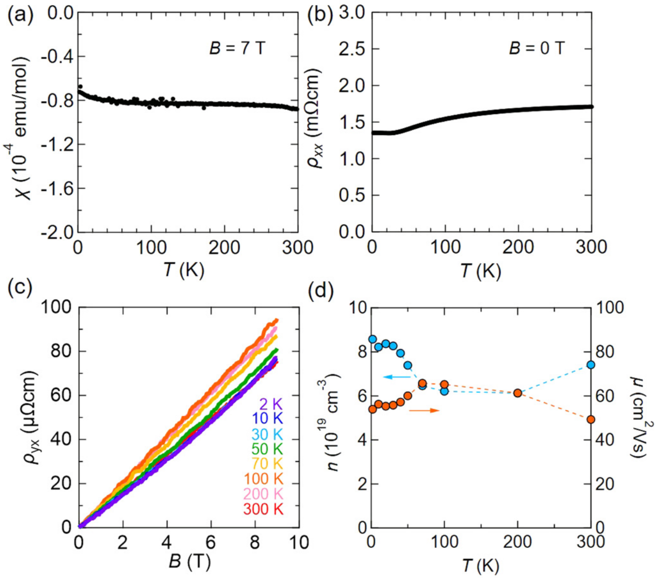

FIG. 4. Magnetic and electronic properties of monoclinic IrSi. (a). Temperature dependence of magnetic susceptibility measured at a magnetic field of $B = 7$ T. (b) Temperature dependence of resistivity measured at $B = 0$ T. (c) Hall resistivity measured at various temperatures. (d) Temperature dependence of carrier density n and mobility μ.

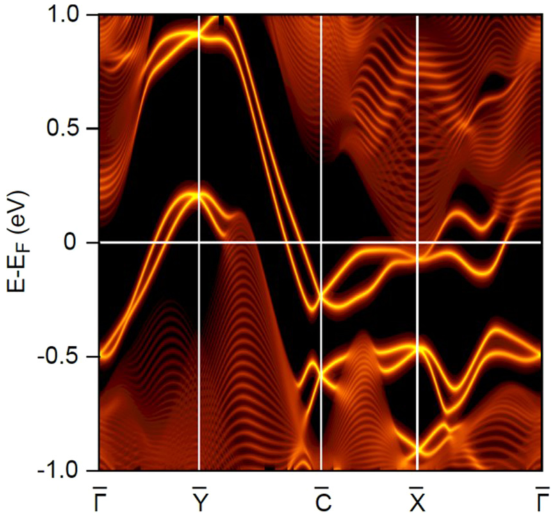

FIG. 5. Surface band structure of monoclinic IrSi showing large Rashba spin splitting. The definition of *k* points is shown in Fig. 3(a).

limited, as exemplified in the high-pressure experiments of CoSn-type materials [17]. The more flexible structures, such as the monoclinic structure we have identified, may be more favorable. Also, there remains a possibility that the FeSi-type phase is realized under HPHT conditions but transforms into the monoclinic phase at ambient atmosphere. The *in situ* x-ray diffraction measurement at HPHT conditions would be necessary to investigate such a possibility. However, we speculate that this is an unlikely scenario, since our calculation on the structural stability (Fig. 2) reveals that the monoclinic structure is more stable than the FeSi-type structure under the present compression range. The monoclinic IrSi shows semimetallic electronic properties with a relatively low carrier density ($\sim 10^{19}/\mathrm{cm}^3$), in accord with the band structure calculations. Fabrication of thin film or heterostructure based on the monoclinic IrSi would be of particular interest, where the surface electronic bands with large Rashba splitting may offer versatile spintronic functionalities [34].

ACKNOWLEDGMENTS

This work was supported by the Joint Usage/Research Center PRIUS, Ehime University (Proposal No. 2018-A45), JSPS KAKENHI (Grants No. JP18K13497, No. JP20H01859, and No. JP20H05155), and JST CREST (Grant No. JPMJCR16F1 and JPMJCR1874).

[1] Y. Imai, M. Mukaida, K. Kobayashi, and T. Tsunoda, Intermetallics **9**, 261 (2001).
[2] K. Göransson, I. Engström, and B. Noläng, J. Alloys Compd. **219**, 107 (1995).
[3] W. L. Korst, L. N. Finnie, and A. W. Searcy, J. Phys. Chem. **61**, 1541 (1957).
[4] S. Mühlbauer, B. Binz, F. Jonietz, C. Pfleiderer, A. Rosch, A. Neubauer, R. Georgii, and P. Böni, Science **323**, 915 (2009).
[5] X. Z. Yu, Y. Onose, N. Kanazawa, J. H. Park, J. H. Han, N. Nagaosa, and Y. Tokura, Nature (London) **465**, 901 (2010).
[6] A. Bauer, A. Neubauer, C. Franz, W. Münzer, M. Garst, and C. Pfleiderer, Phys. Rev. B **82**, 064404 (2010).
[7] G. Chang, S.-Y. Xu, B. J. Wieder, D. S. Sanchez, S.-M. Huang, I. Belopolski, T.-R. Chang, S. Zhang, A. Bansil, H. Lin, and M. Z. Hasan, Phys. Rev. Lett. **119**, 206401 (2017).
[8] P. Tang, Q. Zhou, and S.-C. Zhang, Phys. Rev. Lett. **119**, 206402 (2017).
[9] D. Takane, Z. Wang, S. Souma, K. Nakayama, T. Nakamura, H. Oinuma, Y. Nakata, H. Iwasawa, C. Cacho, T. Kim, K. Horiba, H. Kumigashira, T. Takahashi, Y. Ando, and T. Sato, Phys. Rev. Lett. **122**, 076402 (2019).
[10] D. S. Sanchez, I. Belopolski, T. A. Cochran, X. Xu, J.-X. Yin, G. Chang, W. Xie, K. Manna, V. Süß, C.-Y. Huang, N. Alidoust, D. Multer, S. S. Zhang, N. Shumiya, X. Wang, G-Q. Wang, T.-R. Chang, C. Felser, S.-Y. Xu, S. Jia, H. Lin, and M. Z. Hasan, Nature (London) **567**, 500 (2019).
[11] Z. Rao, H. Li, T. Zhang, S. Tian, C. Li, B. Fu, C. Tang, L. Wang, Z. Li, W. Fan, J. Li, Y. Huang, Z. Liu, Y. Long, C. Fang, H. Weng, Y. Shi, H. Lei, Y. Sun, T. Qian, T. Qian, and H. Ding, Nature (London) **567**, 496 (2019).
[12] J. P. Gambino and E. G. Colgan, Mater. Chem. Phys. **52**, 99 (1998).
[13] H. Elabd and W. F. Kosonocky, RCA Rev. **43**, 569 (1982).
[14] M. Wittmer, Phys. Rev. B **42**, 5249 (1990).
[15] J. A. Hernandez, L. Vočadlo, and I. G. Wood, J. Alloys Compd. **626**, 375 (2015).
[16] V. I. Larchev and S. V. Popova, J. Less-Common Met. **87**, 53 (1982).
[17] A. S. Mikhaylushkin, T. Sato, S. Carlson, S. I. Simak, and U. Häussermann, Phys. Rev. B **77**, 014102 (2008).
[18] F. Izumi and K. Momma, Solid State Phenom. **130**, 15 (2007).
[19] R. Oishi-Tomiyasu, J. Appl. Cryst. **47**, 593 (2014).
[20] L. Schellenberg, J. L. Jorda, and J. Muller, J. Less. Common. Metals **109**, 261 (1985).
[21] J. P. Perdew, K. Burke, and M. Ernzerhof, Phys. Rev. Lett. **77**, 3865 (1996).
[22] Vienna *Ab Initio* Simulation Package, Version 5.3.5 (2014), https://www.vasp.at/.
[23] F. D. Murnaghan, Proc. Natl. Acad. Sci. USA **30**, 244 (1944).
[24] F. Birch, Phys. Rev. **71**, 809 (1947).
[25] F. Birch, J. Geophys. Res. **83**, 1257 (1978).
[26] G. A. Bain and J. F. Berry, J. Chem. Edu. **85**, 532 (2008).
[27] N. B. Brandt and M. V. Razumeenko, J. Exp. Theor. Phys. **12**, 198 (1961).
[28] H. Fukuyama and R. Kubo, J. Phys. Soc. Jpn. **28**, 570 (1970).
[29] I. Souza, N. Marzari, and D. Vanderbilt, Phys. Rev. B **65**, 035109 (2001).
[30] Y. Bychokv and É. I. Rashba, J. Exp. Theor. Phys. Lett. **39**, 78 (1984).
[31] J. Nitta, T. Akazaki, H. Takayanagi, and T. Enoki, Phys. Rev. Lett. **78**, 1335 (1997).
[32] S. LaShell, B. A. McDougall, and E. Jensen, Phys. Rev. Lett. **77**, 3419 (1996).
[33] A. Kimura, E. E. Krasovskii, R. Nishimura, K. Miyamoto, T. Kadono, K. Kanomaru, E. V. Chulkov, G. Bihlmayer, K. Shimada, H. Namatame, and M. Taniguchi, Phys. Rev. Lett. **105**, 076804 (2010).
[34] A. Manchon, H. C. Koo, J. Nitta, S. M. Frolov, and R. A. Duine, Nat. Matter. **14**, 871 (2015).